

Magnetohydrodynamics simulations on graphics processing units

Hon-Cheng Wong^a & Un-Hong Wong^a & Xueshang Feng^b
& Zesheng Tang^a

^a*NAOC-MUST Collaborative Research Laboratory on Lunar and Planetary Exploration, Faculty of Information Technology, Macau University of Science and Technology, Macao SAR, China*

^b*SIGMA Weather Group, State Key Laboratory for Space Weather, Center for Space Science and Applied Research, Chinese Academy of Sciences, Beijing 100190, China*

Abstract

Magnetohydrodynamics (MHD) simulations based on the ideal MHD equations have become a powerful tool for modeling phenomena in a wide range of applications including laboratory, astrophysical, and space plasmas. In general, high-resolution methods for solving the ideal MHD equations are computationally expensive and Beowulf clusters or even supercomputers are often used to run the codes that implemented these methods. With the advent of the Compute Unified Device Architecture (CUDA), modern graphics processing units (GPUs) provide an alternative approach to parallel computing for scientific simulations. In this paper we present, to the authors' knowledge, the first implementation to accelerate computation of MHD simulations on GPUs. Numerical tests have been performed to validate the correctness of our GPU MHD code. Performance measurements show that our GPU-based implementation achieves speedups of 2 (1D problem with 2048 grids), 106 (2D problem with 1024^2 grids), and 43 (3D problem with 128^3 grids), respectively, compared to the corresponding serial CPU MHD implementation.

Key words: MHD simulations, GPUs, CUDA

1 Introduction

Magnetohydrodynamics (MHD) simulations are associated with large spatial ($L > r_i \sim 100$ km) and temporal ($\tau > 1/\omega_i \sim 10$ s) scales [11], where r_i

is the ion gyro-radius and ω_i is the gyro-frequency. The ideal MHD equations treat plasma like a conducting fluid having macroscopic parameters that accurately describe its particle-like interactions by coupling the fluid dynamics equations with the Maxwell's equations. These equations can be used in modeling phenomena in a wide range of applications including laboratory [6], astrophysical [39], and space plasmas [9]. However, they form a nonlinear system of hyperbolic conservation laws, which is so complex and high-resolution methods are necessary to solve them in order to capture shock waves and other discontinuities. These high-resolution methods are in general computationally expensive and parallel computational resources such as Beowulf clusters or even supercomputers are often utilized to run the codes that implemented these methods in a large-scale astrophysical simulation [26] [40] or space weather modeling [13] [34].

In the last few years, the rapid development of graphics processing units (GPUs) makes them more powerful in performance and more programmable in functionality. By comparing the computational power of GPUs and CPUs, GPUs exceed CPUs by orders of magnitude. The theoretical peak performance of the current consumer graphics card NVIDIA GeForce GTX 295 (with two GPUs) is 1788.48G floating-point operations per second (FLOPS) per GPU in single precision while a CPU (Core 2 Quad Q9650 — 3.0 GHz) gives a peak performance of around 96GFLOPS in single precision. The release of the *Compute Unified Device Architecture (CUDA)* [22] hardware and software architecture is the culmination of such development. With CUDA, one can directly exploit a GPU as a data-parallel computing device by programming with the standard C language and avoid working with a high-level shading language such as Cg [19], which requires a significant amount of graphics specific knowledge and was previously used for performing computation on GPUs.

CUDA is a general purpose parallel computing architecture developed by NVIDIA. It includes the CUDA Instruction Set Architecture (ISA) and the parallel compute engine. An extension to C programming language and its compiler are provided, making the parallelism and high computational power of GPUs can be used not only for rendering and shading, but also for solving many computationally intensive problems in a fraction of the time required on a CPU. CUDA also provides basic linear algebra subroutines (CUBLAS) and fast Fourier transform (CUFFT) libraries to leverage GPUs' capabilities. These libraries release developers from rebuilding the frequently used basic operations such as matrix multiplication. Graphics cards from G8x series support the CUDA programming mode; and the latest generation of NVIDIA GPUs (GT2x0 series or later) unifies vertex and fragment processors and provides shared memory for interprocessor communication. For detailed information, we refer the reader to CUDA programming guide [22].

In this paper, we present an implementation to accelerate computation of

MHD simulations on GPUs. To our knowledge, this is the first work describing MHD simulations on GPUs in detail. The goal of our work is to perform a pilot study on numerically solving the ideal MHD equations on GPUs. In addition, the trend of today's chip design is moving to streaming and massively parallel processor models, developing new MHD codes to exploit such architecture is essential. Our GPU MHD code can be easily ported to other many-core platforms such as Intel's upcoming Larrabee [33], making it more flexible for the user's choice of hardware.

This paper is organized as follows: Major applications of scientific computation on GPUs are reviewed in Section 2. The ideal MHD equations and numerical scheme which our GPU MHD code is based on are presented in Section 3. In Section 4, we present the GPU implementation in detail. Numerical tests and performance measurements are given in Section 5 and Section 6, respectively. We conclude our work and point out the future work in Section 7.

2 Scientific Computation on GPUs

Modern GPUs have been utilizing in a variety of scientific applications since C-like programming environments such as Cg [19] and OpenGL shading language [29] were released. These environments provide different levels of control to GPUs but graphics specific knowledge is required in order to develop algorithms on GPUs. For example, in order to drive a GPU to perform arithmetic computation, data should be stored in the form of textures as 32-bit floating point values in the red, green and blue color components of a pixel. In November 2006, NVIDIA released the Compute Unified Device Architecture (CUDA) [22], which provides a new way to implement algorithms on GPUs using standard C language with CUDA extensions without a comprehensive understanding of graphics specific knowledge. The CUDA makes scientific computation on GPUs more convenient and popular in scientific community. In this section, we give a brief review on recent work of scientific applications on GPUs. Two reviews of general-purpose computation on GPUs (GPGPUs) can be found in [24] and [25]. As the techniques for implementing algorithms on GPUs using shading languages and CUDA are quite different, we categorize the GPU-based algorithms into two classes: Shading-language-based and CUDA-based algorithms.

2.1 *Shading-language-based algorithms*

Before the release of CUDA, early implementations of algorithms on GPUs using shading languages basically execute on fragment processors. This is due

to the fact that there are more fragment processors than vertex processors on a GPU and the output from fragment processors can directly be sent to video memory for rendering or visualization.

Tomov *et al.* [43] presented an GPU implementation of Monte Carlo type simulations using Cg [19] on a GPU and obtained a speedup of 3 compared to the CPU version. Yang *et al.* [47] proposed a method to accelerate computation of molecular dynamics on GPUs using Cg and achieved a speedup of 10-11. Portegies Zwart *et al.* [27] developed a code on GPUs for direct gravitational N -body simulations using Cg and compared its performance with the code on the host workstation and the GRAPE-6Af special purpose computer.

There is a limited number of research on using GPUs for solving certain kind of partial differential equations (PDEs). Hagen *et al.* [12] reviewed two classical finite volume schemes including Lax-Friedrichs and Lax-Wendroff as well as a general class of semi-discrete finite volume schemes. These schemes were implemented with Cg on GPUs to solve the Euler equations and the shallow-water equations, which are systems of conservation laws. A speedup of 30-40 was achieved for $N = 1024^2$ problem in their GPU implementations. Sander-son *et al.* [30] proposed a GPU-based approach using Cg for solving PDEs within advection-reaction-diffusion models and obtained a speedup of 22-27.

2.2 CUDA-based algorithms

A increasing number of new GPU implementations with CUDA in different area of scientific simulations have been proposed, some of them were previously implemented on the GPU using Cg and were re-implemented using CUDA while others are new scientific applications on GPUs. Detailed performance studies on GPUs with CUDA can be found in [5] and [31].

Based on their previous work [27], Belleman *et al.* [3] re-implemented the direct gravitational N -body simulations on GPUs using CUDA. For $N \gtrsim 10^5$, they reported a speedup of about 100 compared to the host CPU and about the same speed as the GRAPE-6Af. A library **Sapporo** for performing high precision gravitational N -body simulations was developed on GPUs by Gaburov *et al.* [10]. This library achieved twice as fast as commonly used GRAPE6A/GRAPE6-BLX cards.

Stantchev *et al.* [37] [38] implemented a Particle-In Cell (PIC) code on GPUs for plasmas simulations and visualizations and demonstrated a speedup of 11-22 for different grid sizes. Some new CUDA implementations of molecular dynamics were presented and different acceleration speedups were achieved in recent two years [1] [46] [18] [20]. Inspired by the work of Tomov *et al.* [43], Preis *et al.* [28] implemented Monte Carlo simulations of the two dimensional

ferromagnetic square lattice Ising model and the three dimensional ferromagnetic cubic lattice Ising model on GPUs with CUDA, achieving up to 60 speedups for the 2D Ising model and 30 speedups for the 3D Ising model.

There are two recent studies on solving PDEs on GPUs with CUDA. Elsen *et al.* [7] described a CUDA implementation for the large calculation of the flow over a hypersonic vehicle and over 40x speedups for simple test geometries and 20x speedups for complex geometries were reported, respectively. Klöckner *et al.* [15] described the mapping of discontinuous Galerkin methods onto the CUDA programming model in detail. Their method demonstrated a speedup of 14 to 65. Our work can be considered as one of numerical solution of PDEs methods on GPUs and specific for the ideal MHD equations.

3 Magnetohydrodynamics Simulations

In MHD simulations, the ideal MHD equations with the assumption of the magnetic permeability $\mu = 1$ can be represented as hyperbolic system of conservation laws as follows [11]

$$\frac{\partial \rho}{\partial t} + \nabla \cdot (\rho \mathbf{v}) = 0 \quad (1)$$

$$\frac{\partial \rho \mathbf{v}}{\partial t} + \nabla \cdot (\rho \mathbf{v} \mathbf{v} - \mathbf{B} \mathbf{B}) + \nabla P^* = 0 \quad (2)$$

$$\frac{\partial \mathbf{B}}{\partial t} + \nabla \times (\mathbf{v} \mathbf{B} - \mathbf{B} \mathbf{v}) = 0 \quad (3)$$

$$\frac{\partial E}{\partial t} + \nabla \cdot ((E + P^*) \mathbf{v} - \mathbf{B} (\mathbf{B} \cdot \mathbf{v})) = 0 \quad (4)$$

Here, ρ is the mass density, $\rho \mathbf{v}$ the momentum density, \mathbf{B} the magnetic field, and E the total energy density. The total pressure $P^* \equiv P + \frac{\mathbf{B} \mathbf{B}}{2}$ where P is the gas pressure that satisfies the equation of state, $P \equiv (\gamma - 1)(E - \rho \frac{\mathbf{v} \mathbf{v}}{2} - \frac{\mathbf{B} \mathbf{B}}{2})$. In addition, the MHD equations should obey the divergence-free constraint $\nabla \cdot \mathbf{B} = 0$.

Over the last few decades, there has been a dramatic increase in the number of publications on numerical solution of ideal MHD equations. In particular the development of shock-capturing numerical methods for ideal MHD equations. We do not provide an exhaustive review of the literature here. A comprehensive treatment of numerical solution of MHD equations can be found in [16]. Pen *et al.* [26] proposed a free, fast, simple, and efficient total variation diminishing (TVD) MHD code which features modern high-resolution shock capturing. This code is second-order accuracy in space and time and enforces the $\nabla \cdot \mathbf{B} =$

0 constraint to machine precision. Due to these advantages and convenience for GPU verse CPU comparison, the underlying numerical scheme in our GPU MHD code is based on this work. A detailed comparison of shock capturing MHD codes can be found in [44]. We plan to explore other recent high-order Godunov schemes such as [17] and [41] for GPUs as our future work.

We briefly review the numerical scheme we applied in our GPU MHD code here. The magnetic field is updated in separate two-dimensional advection-constraint steps while holding the fluid variables fixed. In order to keep the $\nabla \cdot \mathbf{B} = 0$ to machine precision, the magnetic field is defined on cell faces [8]. The magnetic field is represented in arrays [26]

$$\begin{aligned} Bx(i, j, k) &= B_{i-1/2, j, k}^x \\ By(i, j, k) &= B_{i, j-1/2, k}^y \\ Bz(i, j, k) &= B_{i, j, k-1/2}^z \end{aligned} \quad (5)$$

where the cell centers are denoted by $(i, j, k) \equiv (x_i, y_j, z_k)$, and faces by $(i \pm 1/2, j, k)$, $(i, j \pm 1/2, k)$, and $(i, j, k \pm 1/2)$, etc. Then we can give the flux out of cell (i, j, k) as [26]

$$\begin{aligned} \left(\int d^3x \nabla \cdot \mathbf{B} \right)_{ijk} &= B_{i+1/2, j, k}^x - B_{i-1/2, j, k}^x \\ &\quad + B_{i, j+1/2, k}^y - B_{i, j-1/2, k}^y \\ &\quad + B_{i, j, k+1/2}^z - B_{i, j, k-1/2}^z \end{aligned} \quad (6)$$

The induction equation can be expressed in spatial component form

$$\frac{\partial B_x}{\partial t} + \frac{\partial}{\partial y} (v_y B_x - B_y v_x) = 0 \quad (7)$$

$$\frac{\partial B_y}{\partial t} + \frac{\partial}{\partial x} (v_x B_y - B_x v_y) = 0 \quad (8)$$

B_x is updated by constructing a second-order-accurate upwind *electromotive force (EMF)* $v_y B_x$ using Jin & Xin's relaxing TVD method [14] in the advection step. Then this same EMF is immediately used to update B_y in the constraint step.

The fluid variables are updated while holding the magnetic fields fixed and interpolated to grid centers with second-order accuracy. Consider advection along the x direction, the ideal MHD equations can be written in flux-conservative form as [26]

$$\frac{\partial \mathbf{u}}{\partial t} + \frac{\partial \mathbf{F}(u)}{\partial x} = 0 \quad (9)$$

where the flux vector is given by

$$\mathbf{F} = \begin{pmatrix} \rho v_x \\ \rho v_x^2 + P^* - B_x^2 \\ \rho v_x v_y - B_x B_y \\ \rho v_x v_z - B_x B_z \\ (E + P^*)v_x - B_x \mathbf{B} \cdot \mathbf{v} \end{pmatrix} \quad (10)$$

and the pressure is $p = (\gamma - 1)(E - \rho v^2/2 - B^2/2)$ and the total pressure is $P^* = p + B^2/2$. Equation (9) is then solved by Jin & Xin's relaxing TVD method [14]. With this method, a new variable $\mathbf{w} = \mathbf{F}(\mathbf{u})/c$ is defined, where $c(x, t)$ is a free positive function called the *flux freezing speed*. For ideal MHD equations, we have $\mathbf{u} = (u_1, u_2, u_3, u_4, u_5) = (\rho, \rho v_x, \rho v_y, \rho v_z, E)$ and equations

$$\frac{\partial \mathbf{u}}{\partial t} + \frac{\partial}{\partial x}(c\mathbf{w}) = 0 \quad (11)$$

$$\frac{\partial \mathbf{w}}{\partial t} + \frac{\partial}{\partial x}(c\mathbf{u}) = 0 \quad (12)$$

These equations can be decoupled through a change of left and right moving variables $\mathbf{u}^R = (\mathbf{u} + \mathbf{w})/2$ and $\mathbf{u}^L = (\mathbf{u} - \mathbf{w})/2$

$$\begin{aligned} \frac{\partial \mathbf{u}^R}{\partial t} + \frac{\partial}{\partial x}(c\mathbf{u}^R) &= 0 \\ \frac{\partial \mathbf{u}^L}{\partial t} - \frac{\partial}{\partial x}(c\mathbf{u}^L) &= 0 \end{aligned} \quad (13)$$

The flux freezing speed c is the maximum speed information can travel and should be set to $|v_x| + (\gamma p/\rho + b^2/\rho)^{1/2}$ as the maximum speed of the fast MHD wave over all directions is chosen. Time integration is implemented using a second-order Runge-Kutta scheme, and the time step is determined by satisfying the CFL condition [26]

$$\begin{aligned} c_{max} &= [\max(|v_x|, |v_y|, |v_z|) + (\gamma p/\rho + \mathbf{B}^2/\rho)^{1/2}] \\ \Delta t &= cfl/c_{max} \end{aligned} \quad (14)$$

where cfl is the Courant-Number and $cfl \lesssim 1$ is generally set to $cfl \simeq 0.7$ for stability.

Extension to three dimensions can be done through a Strang-type directional splitting [42]. Generalization of the relaxing TVD from one-dimensional to three dimensions is summarized in [45]. Equation (9) is dimensionally split into three separate one-dimensional equations. For a time step Δt , let $fluid_x$ be the fluid update along x , $B_{x \rightarrow y}$ be the update of B_x along y , and L_i be the update operator of u^t to $u^{t+\Delta t}$ by including the flux along i direction. Each L_i includes three update operations in sequence, for example, L_x includes $fluid_x$, $B_{y \rightarrow x}$, and $B_{z \rightarrow x}$. A forward sweep and a reverse sweep are defined as $u^{t+\Delta t} = L_z L_y L_x u^t$ and $u^{t+2\Delta t} = L_x L_y L_z u^{t+\Delta t}$, respectively. A complete update combines a forward sweep and reverse sweep. The dimensional splitting of the relaxing TVD can be expressed as follows [45]

$$u^{t_2} = u^{t_1+2\Delta t_1} = L_x L_y L_z L_z L_y L_x u^{t_1} , \quad (15)$$

$$u^{t_3} = u^{t_2+2\Delta t_2} = L_z L_x L_y L_y L_x L_z u^{t_2} , \quad (16)$$

$$u^{t_4} = u^{t_3+2\Delta t_3} = L_y L_z L_x L_x L_z L_y u^{t_3} , \quad (17)$$

where Δt_1 , Δt_2 , and Δt_3 are sequential time steps after each double sweep.

4 GPU Implementation

In this section, we provide the implementation details of our GPU MHD code. In our GPU MHD code, all computations are performed entirely on GPUs and all data is stored in the GRAM of the graphics card.

4.1 Data Storage Arrangement

The most intuitive way to write a parallel program to solve a multidimensional problem is to use multidimensional arrays for data storage and multidimensional threads for computation. However, the ability of the current CUDA does not support multidimensional threads, therefore, we could not implement our code in such a straightforward way. Especially in three dimensions or higher dimensions, there are still some limitations in handling multidimensional arrays and multidimensional threads. As a result, the most primitive way is to store data in one-dimension and perform parallel computation with one-dimension threads. By using an indexing technique, our storage and threading method

can be extended to solve multidimensional problems. Our data storage arrangement is expressed in Fig. 1 and in Equations (18) to (19).

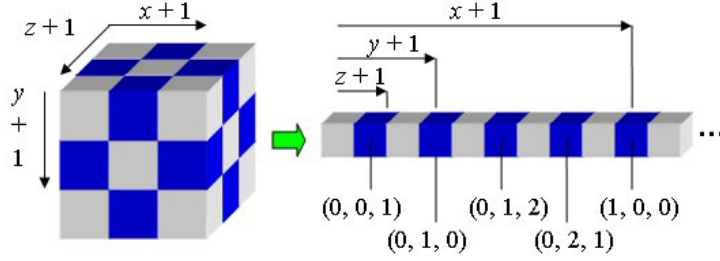


Fig. 1. Mapping from 3D array to 1D array in columns major.

$$\begin{cases} INDEX_x = index / (SIZE_y \times SIZE_z) \\ INDEX_y = [index \bmod (SIZE_y \times SIZE_z)] / SIZE_z \\ INDEX_z = index \bmod SIZE_z \end{cases} \quad (18)$$

$$INDEX_x \pm 1 = index \pm (SIZE_y \times SIZE_z) \quad (19)$$

$$INDEX_y \pm 1 = index \pm SIZE_z \quad (20)$$

$$INDEX_z \pm 1 = index \pm 1 \quad (21)$$

Here $INDEX_x$, $INDEX_y$, and $INDEX_z$ are the indexes of a 3D matrix. $index$ is the 1D index used in our code, $SIZE_y$, and $SIZE_z$ are the matrix size (number of grids in our study) of a 3D matrix.

Equation (18) expresses the mapping of three-dimensional indexes to one-dimensional indexes. Equations (19) to (21) express the shift operations. Shift operations are very important in numerical solution of conservation laws because some calculations are based on the neighboring grids.

4.2 Program Flow

The program flow of our GPU implementation is shown in Fig. 2. After the calculation of the CFL condition, the sweeping operations will be performed. The sweeping operation L_i will update both the fluid variables and orthogonal magnetic fields along i dimension. This is a core computation operation in the relaxing TVD scheme as described in Section 3.

The CFL condition for three-dimensional relaxing TVD scheme is obtained by Equation (14). The procedure is to calculate all the c_{max} of each grid and

find out the maximum value. In our GPU implementation, we used parallel computation power of CUDA to calculate the c_{max} of each grid in parallel and stored all the c_{max} in a matrix. Then we used `cublasIsamax` function to find out the maximum c_{max} of matrix in parallel (called reduction operation). The `cublasIsamax` function is provided in the CUBLAS library — a set of basic operations for vector and matrix provided by NVIDIA with the CUDA toolkit [22]. The implementation of sweeping operations will be explained in the next subsection.

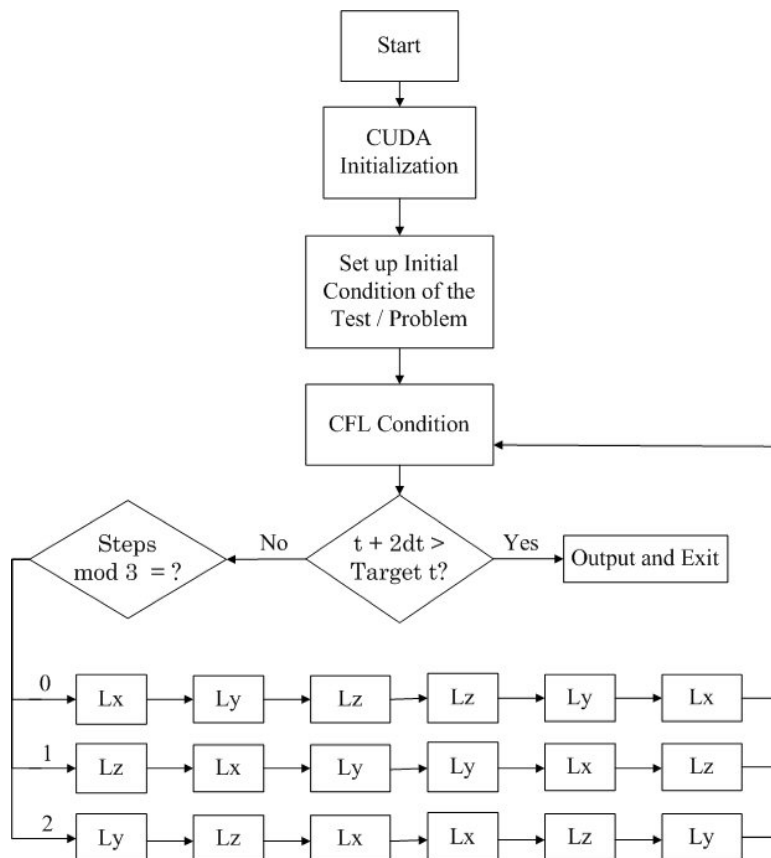


Fig. 2. The flow chat of our GPU MHD code.

4.3 Sweeping Operations

Before we start to describe the sweeping operations, consideration of memory arrangement is presented first in the following.

Implementing parallel computation on CUDA kernels is somewhat similar to parallel implementation on a CPU-cluster, but it is not the same. The major concern is the memory constrain in GPUs. CUDA makes parallel computation process on GPUs which can only access their graphics memory (GRAM).

Therefore, data should be stored in the GRAM in order to be accessed by the GPUs. There are several kinds of memory on graphics hardware including registers, local memory, shared memory, and global memory, etc., and they have different characteristics and usages [22], making memory management of CUDA quite different compared to parallel computation on a CPU-cluster. In addition, even the size of GRAM in a graphics card increases rapidly in newer models (for example, the latest NVIDIA graphics card — GeForce GTX 295 has 1.75G GRAM), but not all the capacity of GRAM can be used to store data arbitrarily. Shared memory and local memory are flexible to use, however, their sizes are very limited in a block and thus they cannot be used for storing a large size of data. In general, numerical solution of conservation laws will generate many intermediate results during the computation process, these results should be stored for subsequent steps of the process. Therefore, global memory was mainly used in our GPU MHD code.

After the maximum value of c_{max} in Equation (14) is found, we can get the Δt by determining the Courant-Number (cfl). The sequential step is the calculation of L_i ($i = x, y, z$ in our implementation). The implementation of L_i includes two parts: update the fluid variables and update orthogonal magnetic fields. As an example, the process for calculating L_x is shown in Fig. 3 where each block was implemented with one or several CUDA kernels (function run on the CUDA/GPU [22]). The process for calculating L_y or L_z is almost the same except that the dimension indexes are different.

The first part of the L_x calculation process is to update the fluid variables. In this process, we have to calculate the magnetic fields of the cell first because all the magnetic fields are defined on the faces of the cell [26]. To update the fluid variables of L_x , the main process is to calculate the affect of the orthogonal magnetic fields to the fluid variables of Equation (10) — one process gives the flux of in the step of $\Delta t/2$. As we mentioned before, numerical solution of conservation laws needs lots of memory because there are many intermediate results generated during the computation process. These intermediate results should be stored for the next calculation step which needs the information of the neighboring grids obtained in the previous calculation step. Otherwise, in order to avoid the asynchronous problem in parallel computation, we have to do many redundant processes — calculating all the neighboring grids for updating the fluid and magnetic orthogonal magnetic fields of each grid. That means each grid has to be calculated repeatedly. With the purpose to minimizing the memory usage, we divided the calculation process of L_x into several steps.

The second part of the L_x calculation process is to update the orthogonal magnetic fields in y -dimension and z -dimension with the fluid along x -dimension. The strategy and implementation are similar to those in the first part but with a different algorithm for the orthogonal magnetic fields. The processes dealing

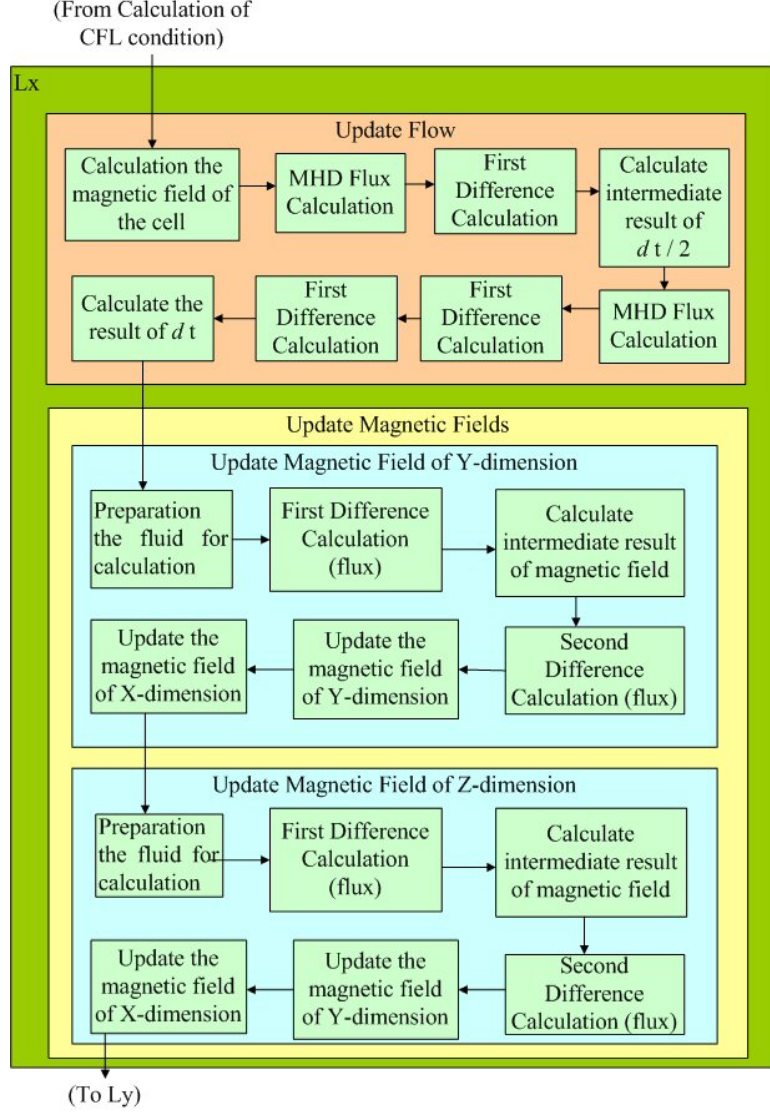


Fig. 3. Calculation process of L_x .

with the “differences calculation” are also divided into several steps to minimize the storage of the intermediate results and guarantee there is no wrong results caused by asynchronous problem. It should be realized that most of the processes in the three-dimensional relaxing TVD scheme with the dimensional splitting technique is similar. Pen *et al.* [26] swapped the data of x , y , and z -dimensions while our implementation used one-dimensional arrays. But the similar swapping technique can be applied in our case with some indexing operations. Instead of transposing or swapping the data, we implemented the flux computation with two kernels, one is for the indexing operations, and other one is for the calculation of the relaxing TVD scheme. Therefore, the difference among L_x , L_y , and L_z is the dimensional index and the flux computation of our implementation is shown in Fig. 4.

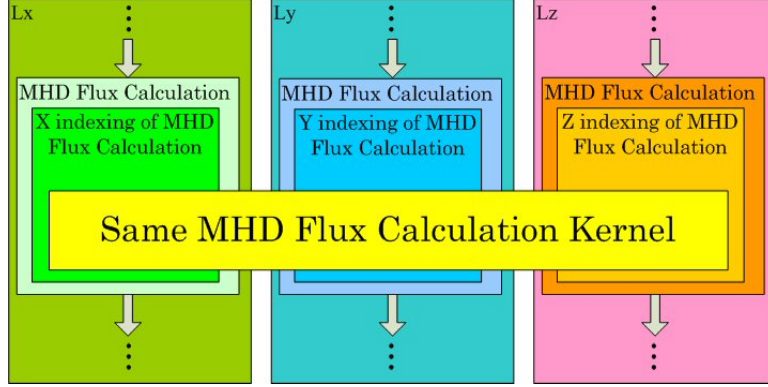


Fig. 4. Flux computation in our implementation.

The indexing operation swaps the target that will be updated and the neighboring relationship will also be changed accordingly. For example, the calculation that uses $x + 1$ as the neighboring element in L_x will be changed to $y + 1$ in L_y . As transposing the data in a matrix needs more processing time, it is flexible and efficient to extend the code to multidimensional by dividing the indexing operations and flux calculation.

After the whole pipeline of Fig. 2 is completed, the MHD simulation results will be stored in the GRAM and these results are readily to be further processed by the GPUs for visualization or read back to the CPU for other usage.

5 Numerical Tests

In this section, several numerical tests for validation of our GPU MHD code are given.

5.1 One-Dimensional Brio-Wu Shock Tube Problem

One-dimensional Brio-Wu shock tube problem [4] which is a MHD version of the Sod problem [35], consists of a shock tube with two initial equilibrium states as follows

Left side ($x < 0.5$)

$$\left\{ \begin{array}{c} v_x \\ v_y \\ v_z \end{array} \right\} = \left\{ \begin{array}{c} 0 \\ 0 \\ 0 \end{array} \right\} \quad (22)$$

$$\begin{pmatrix} B_x \\ B_y \\ B_z \end{pmatrix} = \begin{pmatrix} 0.75 \\ 1 \\ 0 \end{pmatrix} \quad (23)$$

$$\rho = 1, \quad p = 1 \quad (24)$$

Right side ($x \geq 0.5$)

$$\begin{pmatrix} v_x \\ v_y \\ v_z \end{pmatrix} = \begin{pmatrix} 0 \\ 0 \\ 0 \end{pmatrix} \quad (25)$$

$$\begin{pmatrix} B_x \\ B_y \\ B_z \end{pmatrix} = \begin{pmatrix} 0.75 \\ -1 \\ 0 \end{pmatrix} \quad (26)$$

$$\rho = 0.125, \quad p = 0.1 \quad (27)$$

Constant value of $\gamma = 2$ was used and the problem was solved for $x \in [0, 1]$ with 1024 grids. Numerical results are presented at $t = 0.08L$ in Fig. 5, which includes the density, the pressure, the energy, the y -magnetic field components, and the x - and y -velocity components. The results are in agreement with those obtained by Brio and Wu [4] and Zachary *et al.* [48].

5.2 Two-dimensional Orszag-Tang Problem

Orszag-Tang problem [23] is used to study incompressible MHD turbulence. In our test, the boundary conditions are periodic everywhere. The density ρ , pressure p , initial velocities (v_x, v_y, v_z) , and magnetic field (B_x, B_y, B_z) are given by

$$\begin{pmatrix} v_x \\ v_y \\ v_z \end{pmatrix} = \begin{pmatrix} -\sin(2\pi y) \\ \sin(2\pi x) \\ 0 \end{pmatrix} \quad (28)$$

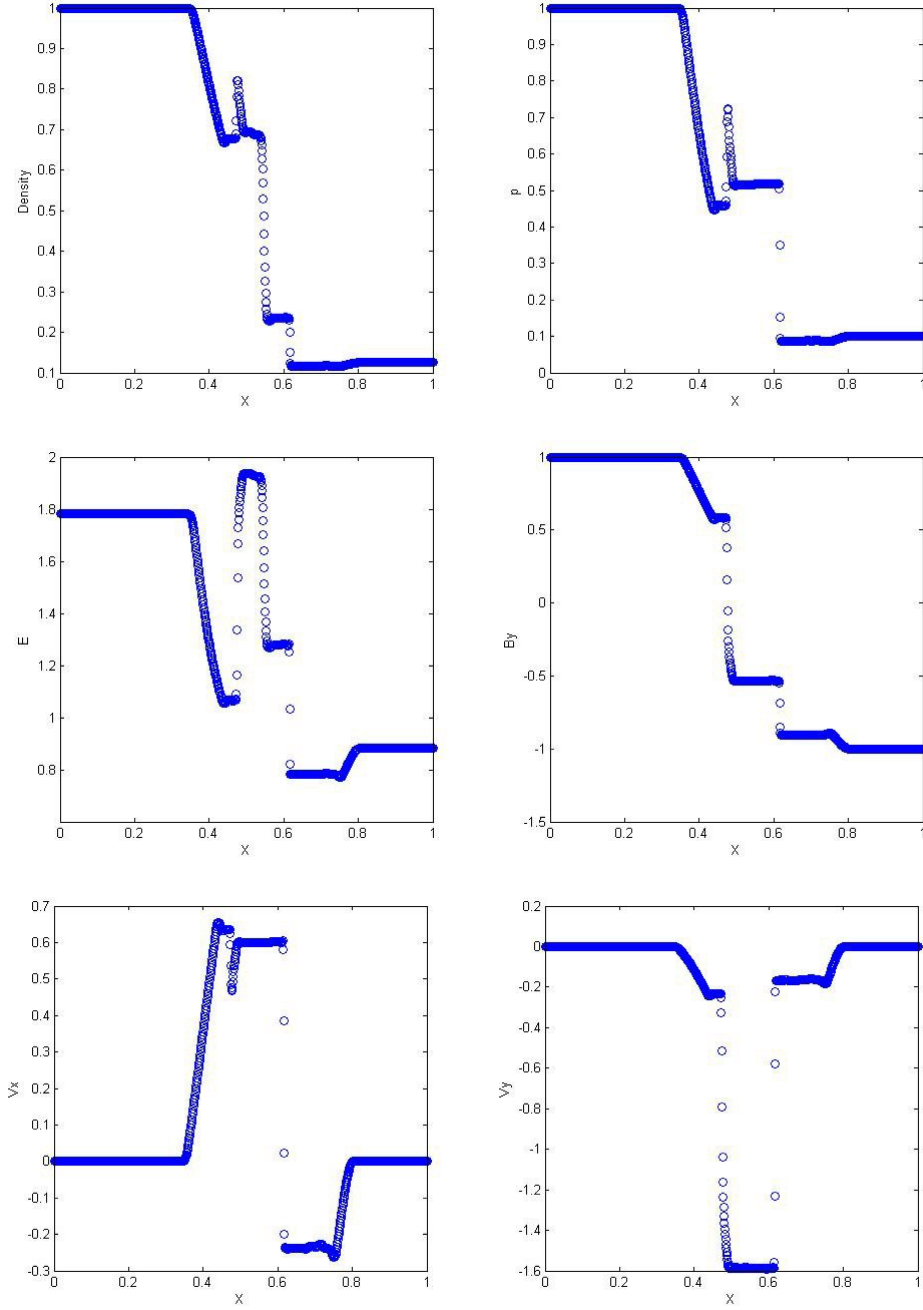


Fig. 5. Results of Brio-Wu shock tube problem at $t = 0.08L$ computed with 1024 grids.

$$\begin{Bmatrix} B_x \\ B_y \\ B_z \end{Bmatrix} = \begin{Bmatrix} -B_0 \sin(2\pi y) \\ B_0 \sin(4\pi x) \\ 0 \end{Bmatrix} \quad \text{where } B_0 = 1/\sqrt{4\pi} \quad (29)$$

$$\rho = 25/(36\pi), \quad p = 5/(12\pi), \quad \gamma = 5/3, \quad (0 \leq x \leq 1) \quad (0 \leq y \leq 1) \quad (30)$$

The Orszag-Tang vortex test was performed in a two-dimensional periodic box with 512×512 grids. The results of the density and gas pressure evolution of the Orszag-Tang problem at $t = 0.5L$ and $t = 1.0L$ are shown in Fig. 6, where the complex pattern of interacting waves is perfectly recovered. The results agree well with those in Lee *et al.* [17].

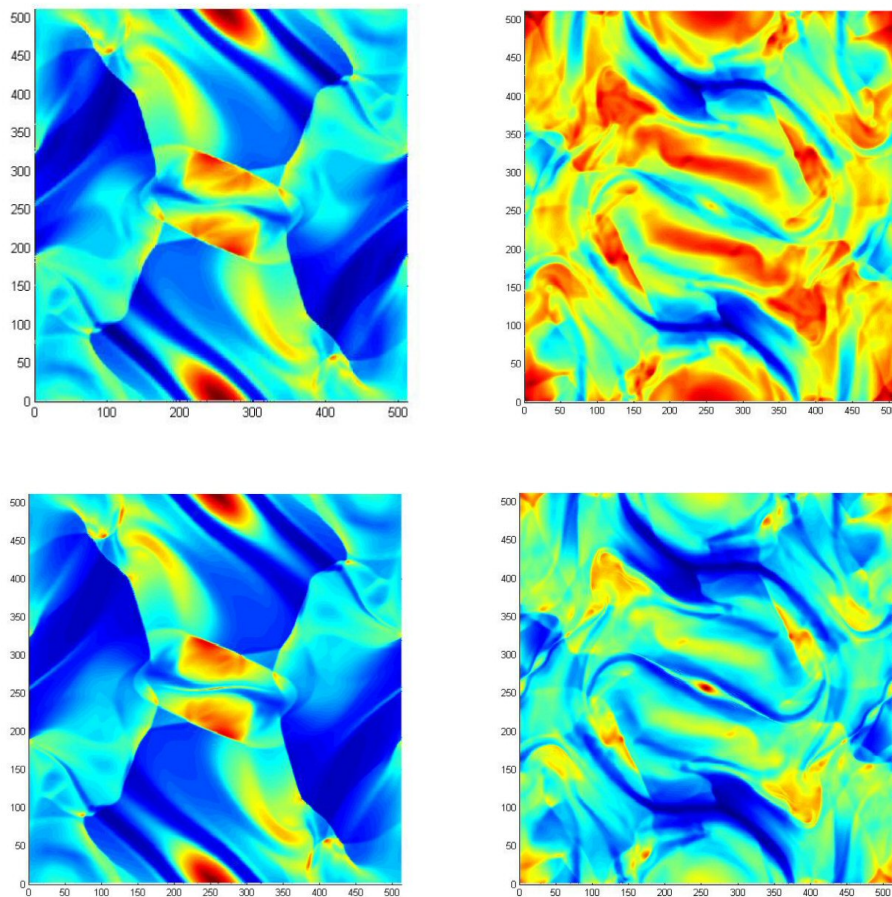


Fig. 6. Results of the density (top) and gas pressure (bottom) of Orszag-Tang vortex test at $t = 0.5L$ (left) and $t = 1.0L$ (right) computed with 512×512 grids.

5.3 Two-Dimensional Blast Wave Problem

The second 2D test is MHD blast wave problem. The MHD spherical blast wave problem of Zachary *et al.* [48] is initiated by an over pressured region in the center of the domain. The result is a strong outward moving spherical shock with rarified fluid inside the sphere. The condition for 2D MHD blast

wave problem is listed as follows [36]

$$\begin{pmatrix} v_x \\ v_y \\ v_z \end{pmatrix} = \begin{pmatrix} 0 \\ 0 \\ 0 \end{pmatrix} \quad (31)$$

$$\begin{pmatrix} B_x \\ B_y \\ B_z \end{pmatrix} = \begin{pmatrix} 1/\sqrt{2} \\ 1/\sqrt{2} \\ 0 \end{pmatrix} \quad (32)$$

$$p = \begin{cases} 10 & \text{inside the spherical region} \\ 0.1 & \text{outside the spherical region} \end{cases} \quad (33)$$

$$\begin{aligned} \rho &= 1, \quad p = 5/(12\pi), \quad \gamma = 5/3 \\ \text{spherical region center} &= (0.5, 0.5), \quad r = 0.1 \\ (0 \leq x \leq 1) \quad (0 \leq y \leq 1) \end{aligned} \quad (34)$$

In Fig. 7, we present images of the density, gas pressure, and magnetic pressure sliced along the $y = 0$ plane at $t = 0.2L$ computed with 512×512 grids. The results are in excellent agreement with those presented in [36].

5.4 Three-Dimensional Blast Wave Problem

The 3D version of MHD spherical blast wave problem was also tested. The condition is listed as follows [36]

$$\begin{pmatrix} v_x \\ v_y \\ v_z \end{pmatrix} = \begin{pmatrix} 0 \\ 0 \\ 0 \end{pmatrix} \quad (35)$$

$$\begin{pmatrix} B_x \\ B_y \\ B_z \end{pmatrix} = \begin{pmatrix} 1/\sqrt{3} \\ 1/\sqrt{3} \\ 1/\sqrt{3} \end{pmatrix} \quad (36)$$

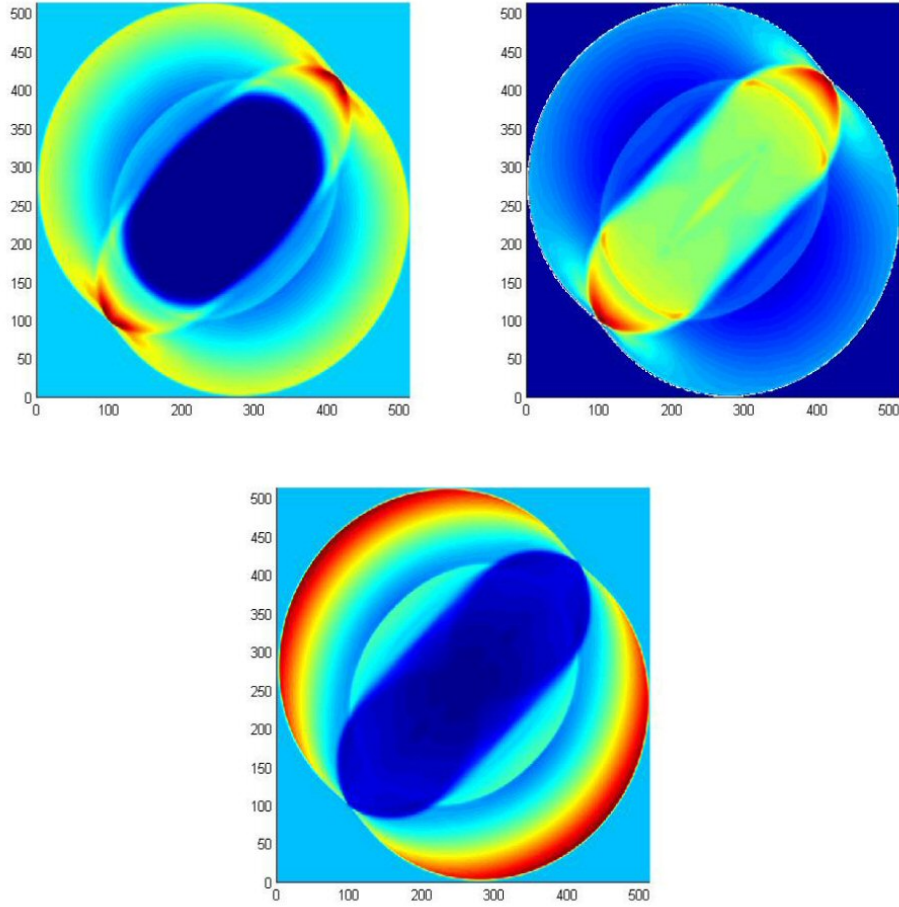


Fig. 7. Results of the density (top-left), gas pressure (top-right) and magnetic pressure (bottom) of the 2D blast wave test at $t = 0.2L$, computed with 512×512 grids.

$$p = \begin{cases} 10 & \text{inside the spherical region} \\ 0.1 & \text{outside the spherical region} \end{cases} \quad (37)$$

$$\rho = 1, \quad \gamma = 5/3$$

$$\text{spherical region center} = (0.5, 0.5, 0.5), \quad r = 0.1 \quad (38)$$

$$(0 \leq x \leq 1) \quad (0 \leq y \leq 1) \quad (0 \leq z \leq 1)$$

Fig. 8 shows the results of 3D blast wave problem, which includes the density, gas pressure, and magnetic pressure at $t = 0.1L$ sliced along x - y plane at $z = 0.5$. The test was computed with $128 \times 128 \times 128$ grids. Due to the scarcity of published 3D test results, we do not make direct contact with results presented in the literature here.

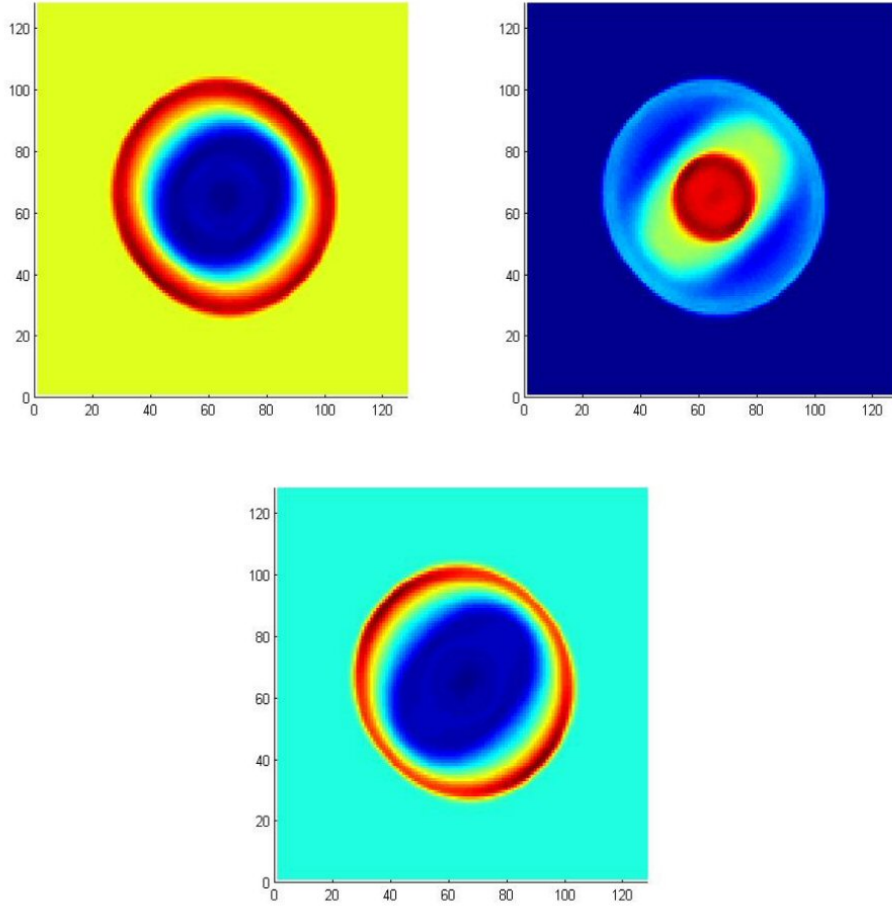


Fig. 8. Results of the density (top-left), gas pressure (top-right) and magnetic pressure (bottom) of 3D blast wave test at $t = 0.1L$ sliced along $x-y$ plane at $z = 0.5$ and computed with $128 \times 128 \times 128$ grids.

6 Performance Measurements

The performance measurements of the GPU and CPU implementations are carried out in this section. Alfvén waves with different number of grids and different dimension were used in the performance tests. We run both our CUDA/GPU MHD code and Pen *et al.*'s FORTRAN/CPU MHD code [26] to perform the simulations of Alfvén waves at $t = 25L$ on a PC with Intel Core i7 965 3.20 GHz CPU, 6G main memory, running Microsoft Windows XP 64-bit Professional. The graphics card is NVIDIA Geforce GTX 295 with 1.75G video memory. Our GPU MHD code was designed for three-dimensional problems, thus the dimensions shown in Tables 1, 2, and 3 are expressed in three-dimensional form.

Table 1 reports the comparison of our CUDA/GPU code and the FORTRAN/CPU code of 1D Alfvén waves test with different number of grids. Basically there

is no speedup when the grid number is 128. When the grid number is 2048, speedup of twice is obtained.

Table 1

The performance results of 1D Alfven waves test

| Number of Grids | CUDA/GPU (ms) | FORTRAN/CPU (ms) | Speedup |
|--------------------------|---------------|------------------|---------|
| $128 \times 1 \times 1$ | 235 | 250 | 1.064 |
| $256 \times 1 \times 1$ | 304 | 484 | 1.592 |
| $512 \times 1 \times 1$ | 429 | 969 | 2.259 |
| $1024 \times 1 \times 1$ | 1538 | 1954 | 1.270 |
| $2048 \times 1 \times 1$ | 1952 | 3906 | 2.001 |

The comparison of our CUDA/GPU code and the FORTRAN/CPU code of 2D Alfven waves test with different number of grids is present in Table 2. In 2D case, a significant performance improvement is observed, especially when the grid number is 512^2 or 1024^2 , a speedup of around 100 is achieved.

Table 2

The performance results of 2D Alfven waves test

| Number of Grids | CUDA/GPU (ms) | FORTRAN/CPU (ms) | Speedup |
|-----------------------------|---------------|------------------|---------|
| $64 \times 64 \times 1$ | 1184 | 5078 | 4.289 |
| $128 \times 128 \times 1$ | 1535 | 20203 | 13.162 |
| $256 \times 256 \times 1$ | 1845 | 80968 | 43.885 |
| $512 \times 512 \times 1$ | 3146 | 322281 | 102.442 |
| $1024 \times 1024 \times 1$ | 12198 | 1293422 | 106.036 |

Table 3 shows the comparison of our CUDA/GPU code and the FORTRAN/CPU code of 3D Alfven waves test with different number of grids. The performance of our CUDA/GPU code is faster than the FORTRAN/CPU code about 33 times and 43 times when the grid number is 64^3 and 128^3 , respectively.

Table 3

The performance results of 3D Alfven waves test

| Number of Grids | CUDA/GPU (ms) | FORTRAN/CPU (ms) | Speedup |
|-----------------------------|---------------|------------------|---------|
| $16 \times 16 \times 16$ | 1231 | 2881 | 2.340 |
| $32 \times 32 \times 32$ | 2066 | 16563 | 8.017 |
| $64 \times 64 \times 64$ | 3697 | 124953 | 33.789 |
| $128 \times 128 \times 128$ | 21774 | 948297 | 43.552 |

The performance tests show that when the number of grids of the test problems is small, such as those in 1D case, our GPU MHD code could not give a significant performance improvement. This is because some processing time was spent when the initialized data and the necessary parameters were copied to the GRAM in the initialization status. When the number of grids increases, an obvious disparity of performance becomes clear, especially for multidimensional cases (see Table 2 and Table 3). For example, in Table 2, our CUDA/GPU implementation even obtained a speedup of around 100 compared to the FORTRAN/CPU implementation when the number of grids is $512 \times 512 \times 1$ or $1024 \times 1024 \times 1$. The performance results show that CUDA is an attractive parallel computing environment for MHD simulations.

7 Conclusion and Future Work

In this paper, we present an implementation to accelerate computation of MHD simulations on GPUs. Numerical tests validate the correctness of our GPU MHD code. Performance measurements show that our GPU-based implementation achieves speedups of 2 (1D problem with 2048 grids), 106 (2D problem with 1024^2 grids), and 43 (3D problem with 128^3 grids), respectively, compared to the corresponding serial CPU MHD implementation. These speedups are promising and indicate an attractive alternative way to perform MHD simulations for higher dimensional problems on GPUs.

There are three directions in our future work, firstly, we are going to extend our GPU MHD code for multiple GPUs and GPU cluster [32] to fully exploit the power of GPUs. Secondly, we will investigate implementing other recent high-order Godunov MHD algorithms such as [17] and [41] on GPUs. Thirdly, as the output of the MHD simulations is already resided in the video memory of the GPU and therefore they can be directly rendered with the GPU using a shading language such as Cg [19], we will explore the three-dimensional (3D) visualization techniques for MHD simulations [21] [38]. These GPU-based algorithms and visualization techniques will be served as the base of our GPU framework for simulating large-scale MHD problems in space weather modeling. With this framework, the MHD simulations and visualizations can be done on GPUs entirely.

8 Acknowledgments

This work has been supported by the Science and Technology Development Fund of Macao SAR under grant 003/2008/A1. The authors would like to

thank Dr. Ue-Li Pen and Bijia Pang at the Canadian Institute for Theoretical Astrophysics, University of Toronto for providing the FORTRAN MHD code.

References

- [1] J. A. Anderson, C. D. Lorenz, A. Travasset, General purpose molecular dynamics simulations fully implemented on graphics processing units, *J. Comput. Phys.* **227** (2008) 5342-5359.
- [2] J. Balbás, E. Tadmor, C.-C. Wu, Non-oscillatory central schemes for one- and two-dimensional MHD equations: I, *J. Comput. Phys.* **201** (2004) 261-285.
- [3] R. G. Belleman, J. Bédorf, S. F. Portegies Zwart, High performance direct gravitational N-body simulations on graphics processing units II: an implementation in CUDA, *New Astronomy* **13** (2008) 103-112.
- [4] M. Brio, C. C. Wu, An upwind differencing scheme for the equations of ideal magnetohydrodynamics, *J. Comput. Phys.* **75** (1988) 400-422.
- [5] S. Che, M. Boyer, J. Meng, D. Tarjan, J. W. Sheaffer, K. Skadron, A performance study of general-purpose applications on graphics processors using CUDA, *J. Parallel Distrib. Comput.* **68** (2008) 1370-1380.
- [6] A. Ciardi, S. Lebedev, A. Frank, E. Blackman, D. Ampleford, C. Jennings, J. Chittenden, T. Lery, S. Bland, S. Bott, G. Hall, J. Rapley, F. Vidal, A. Marocchino, 3D MHD simulations of laboratory plasma jets, *Astrophysics and Space Science* **307** (2007) 17-22.
- [7] E. Elsen, P. LeGresley, E. Darve, Large calculation of the flow over a hypersonic vehicle using a GPU, *J. Comput. Phys.* **227** (2008) 10148-10161.
- [8] C. R. Evans, J. F. Hawley, Simulation of Magnetohydrodynamic flow: a constrained transport method, *Astrophys. J.* **332** (1988) 659-677.
- [9] X. Feng, Y. Zhou, S. T. Wu, A novel numerical implementation for solar wind modeling by the modified conservation element/solution element method, *Astrophys. J.* **655**, (2007) 1110-1126.
- [10] E. Gaburov, S. Harfst, S. P. Zwart, SAPPORO: a way to turn your graphics cards into a GRAPE-6, *New Astronomy* **14** (2009) 630-637.
- [11] J. P. Goedbloed, S. Poedts, *Principles of Magnetohydrodynamics: With Applications to Laboratory and Astrophysical Plasmas*, Cambridge University Press, 2004.
- [12] T. R. Hagen, M. O. Henriksen, J. M. Hjelmervik, K.-A. Lie, How to solve systems of conservation laws numerically using the graphics processor as a high-performance computational engine, in: G. Hasle et al. (Eds.), *Geometric Modelling, Numerical Simulation, and Optimization*, Springer, pages 211-267, 2007.

- [13] Y. Hu, X. Feng, S. T. Wu, W. Song, Three-dimensional MHD modeling of the global corona throughout solar cycle 23, *J. Geophys. Res.* **113** (2008) A03106.
- [14] S. Jin, Z. Xin, The relaxation schemes for systems of conservation laws in arbitrary space dimensions, *Commun. Pure Appl. Math.* **48** (1995) 235-276.
- [15] A. Klöckner, T. Warburton, J. Bridge, J. S. Hesthaven, Nodal discontinuous Galerkin methods on graphics processors, *J. Comput. Phys.* (2009), accepted.
- [16] A. G. Kulikovskii, N. V. Pogorelov, A. Yu. Semenov, *Mathematical Aspects of Numerical Solution of Hyperbolic Systems*, CRC Press, 2001.
- [17] D. Lee, A. E. Deane, An unsplit staggered mesh scheme for multidimensional magnetohydrodynamics, *J. Comput. Phys.* **228** (2009) 952-975.
- [18] W. Liu, B. Schmidt, G. Voss, W. Müller-Wittig, Accelerating molecular dynamics simulations using graphics processing units with CUDA, *Comput. Phys. Commun.* **179** (2008) 634-641.
- [19] W. R. Mark, R. S. Glanville, K. Akeley, M. J. Kilgard, Cg: a system for programming graphics hardware in a C-like language, *ACM Trans. Graph.* **22** (2003) 896-907.
- [20] P. Martinsen, J. Blaschke, R. Künnemeyer, R. Jordan, Accelerating Monte Carlo simulations with an NVIDIA graphics processor, *Comput. Phys. Commun.* (2009), accepted.
- [21] P. Mininni, E. Lee, A. Norton, J. Clyne, Flow visualization and field line advection in computational fluid dynamics: application to magnetic fields and turbulent flows, *New J. Phys.* **10** (2008) 125007.
- [22] NVIDIA Cororation, NVIDIA CUDA Compute Unified Device Architecture Programming Guide 2.2.1, May 2009, <http://www.nvidia.com/cude>.
- [23] A. Orszag, C. M. Tang, Small-scale structure of two-dimensional magneto-hydrodynamics turbulence, *J. Fluid Mech.* **90** (1979) 129-143.
- [24] J. D. Owens, D. Luebke, N. Govindaraju, M. Harris, J. Krüger, A. E. Lefohn, T. Purcell, A survey of general-purpose computation on graphics hardware, *Comput. Graph. Forum* **26** (2007) 80-113.
- [25] J. D. Owens, M. Houston, D. Luebke, S. Green, J. E. Stone, J. C. Phillips, GPU computing, *Proceedings of the IEEE* **96** (2008) 879-899.
- [26] U.-L. Pen, P. Arras, S. Wong, A free, fast, simple and efficient TVD MHD code, *Astrophys. J. Supp.* **149** (2003) 447-455.
- [27] S. F. Portegies Zwart, R. G. Belleman, P. M. Geldof, High-performance direct gravitational N-body simulations on graphics processing units, *New Astronomy* **12** (2007) 641-650.
- [28] T. Preis, P. Virnau, W. Paul, J. J. Schneider, GPU accelerated Monte Carlo simulation of the 2D and 3D Ising model, *J. Comput. Phys.* **228** (2009) 4468-4477.

- [29] R. J. Rost, *OpenGL Shading Language*, Second Edition, Addison-Wesley, 2006.
- [30] A. R. Sanderson, M. D. Meyer, R. M. Kirby, C. R. Johnson, A framework for exploring numerical solutions of advection-reaction-diffusion equations using a GPU-based approach, *Comput. Visual. Sci.* **12** (2009) 155-170.
- [31] O. Schenk, M. Christen, H. Burkhart, Algorithmic performance studies on graphics processing units, *J. Parallel Distrib. Comput.* **68** (2008) 1360-1369.
- [32] H.-Y. Schive, C.-H. Chien, S.-K. Wong, Y.-C. Tsai, T. Chiueh, Graphic-card cluster for astrophysics (GraCCA) — performance tests, *New Astronomy* **13** (2008) 418-435.
- [33] L. Seiler, D. Carmean, E. Sprangle, T. Forsyth, M. Abrash, P. Dubey, S. Junkins, A. Lake, J. Sugerma, R. Cavin, R. Espasa, E. Grochowski, T. Juan, P. Hanrahan, Larrabee: a many-core x86 architecture for visual computing, *ACM Trans. Graph.* **27** (2008) Article 18.
- [34] F. Shen, X. Feng, S. T. Wu, C. Xiang, Three-dimensional MHD simulation of CMEs in three-dimensional background solar wind with the self-consistent structure on the source surface as input: numerical simulation of the January 1997 Sun-Earth connection event, *J. Geophys. Res.* **112** (2007) A06109.
- [35] G. Sod, A survey of several finite difference methods for systems of nonlinear hyperbolic conservation laws, *J. Comput. Phys.* **27** (1978) 1-31.
- [36] Spherical blast wave test page of Athena3D test suite: <http://www.astro.virginia.edu/VITA/ATHENA/blast.html>.
- [37] G. Stantchev, W. Dorland, N. Gumerov, Fast parallel particle-to-grid interpolation for plasma PIC simulations, *J. Parallel Distrib. Comput.* **68** (2008) 1339-1349.
- [38] G. Stantchev, D. Juba, W. Dorland, A. Varshney, Using graphics processors for high-performance computation and visualization of plasma turbulence, *Computing in Science and Engineering* **11** (2009) 52-59.
- [39] J. Stone, T. a. Gardiner, Recent progress in astrophysical MHD, *Comput. Phys. Commun.* **177** (2007) 257-259.
- [40] J. Stone, T. A. Gardiner, P. Teuben, J. F. Hawley, J. B. Simon, Athena: a new code for astrophysical MHD, *Astrophys. J. Supp.* **178** (2008) 137-177.
- [41] J. Stone, T. Gardiner, A simple unsplit Godunov method for multidimensional MHD, *New Astronomy* **14** (2009) 139-148.
- [42] G. Strang, On the construction and comparison of difference schemes, *SIAM J. Numer. Anal.* **5** (1968) 506-517.
- [43] S. Tomov, M. McGuigan, R. Bennett, G. Smith, J. Spiletic, Benchmarking and implementation of probability-based simulations on programmable graphics card, *Comput. Graph.* **29** (2005) 71-80.

- [44] G. Tóth, The $\nabla \cdot \mathbf{B} = 0$ constraint in shock-capturing magnetohydrodynamics codes, *J. Comput. Phys.* **161** (2000) 605-656.
- [45] H. Trac, U.-L. Pen, A primer on Eulerian computational fluid dynamics for astrophysics, *Publications of the Astronomical Society of the Pacific* **115** (2003) 303-321.
- [46] J. A. van Meel, A. Aronld, D. Frenkel, S. F. Portegies Zwart, R. G. Belleman, Harvesting graphics power for MD simulations, *Molecular Simulation* **34** (2008) 259-266.
- [47] J. Yang, Y. Wang, Y. Chen, GPU accelerated molecular dynamics simulation of thermal conductivities, *J. Comput. Phys.* **221** (2007) 799-804.
- [48] A. Zachary, A. Malagoli, P. Colella, A higher-order Godunov method for multidimensional ideal magnetohydrodynamics, *SIAM J. Sci. Comput.* **15** (1994) 263-284.